文章编号：1001-9014(2021)04-0508-08

DOI:10.11972/j.issn.1001-9014.2021.04.010

Dispersion engineered ZnSe rib waveguide for mid-infrared supercontinuum generation

FANG Yi-Ming[1,2], YANG Zhen[1,2], XU Pei-Peng[1,2], YAN Kun-Lun[1,2], SHENG Yan[1,2], WANG Rong-Ping[1,2,3*]

(1. Laboratory of Infrared Materials and Devices, Ningbo University, Ningbo 315211, China;
2. Key Laboratory of Photoelectric Detection Materials and Devices of Zhejiang Province, Ningbo 315211, China;
3. Laboratory of Silicate Materials Science and Engineering, Wuhan University of Technology, Wuhan 430070, China)

Abstract: Mid-infrared supercontinuum generation in dispersion-engineered ZnSe rib waveguides was investigated for the first time. Numerical results showed that the zero-dispersion wavelength can be shifted to a shorter wavelength by adjusting structural parameters and refractive index contrast between the core and cladding layers in the waveguide. The optical field can be well confined in the 4- and 8-μm wide waveguides with a 2-μm thick cladding layer of $Ge_5As_{10}S_{85}$ glass. The effect of waveguide parameters on the bandwidth of the supercontinuum spectrum at a 5-cm-long waveguide was also simulated to understand the effect of the pump wavelength and structure parameters on the supercontinuum generation. Our results showed that supercontinuum output could vary over a wide range depending on structural parameters of the waveguide, the pump power and wavelength. An ultrabroad supercontinuum spectrum from 3.0 up to 12.2 μm (> 2 octaves) was confirmed in a 4 μm-width waveguide with a peak pump power of 20 kW and a pump wavelength of 4.5 μm, which is promising as one of the on-chip supercontinuum light sources for many applications such as biomedical imaging, and environmental and industrial sensing in the mid-infrared.

Key words: ZnSe rib waveguides, supercontinuum, soliton self-frequency, dispersion-engineered

基于色散调制硒化锌脊形波导产生超连续谱

方依明[1,2], 杨 振[1,2], 徐培鹏[1,2], 严昆仑[1,2], 盛 燕[1,2], 王荣平[1,2,3*]

(1. 宁波大学 红外材料与器件实验室, 浙江 宁波 315211;
2. 宁波大学 浙江省光电探测材料与器件重点实验室, 浙江 宁波 315211;
3. 武汉理工大学 硅酸盐材料科学与工程实验室, 湖北 武汉 430070)

摘要: 研究了基于色散调制硒化锌脊形波导中红外超连续谱的产生, 仿真表明通过调整波导中波导芯层和包层之间的折射率差距和结构参数, 零色散波长可以转移到更短的波长。用 2 μm 厚的 $Ge_5As_{10}S_{85}$ 玻璃作为包层, 可以将光场限制在 4 和 8 μm 宽的波导中。为了解泵浦波长和结构参数对超连续谱产生的影响, 模拟 5 cm 长波导在不同条件下产生的超连续谱。我们的结果表明, 泵浦波长和功率以及波导参数是影响超连续谱展宽的主要原因。研究发现, 4 μm 宽硒化锌波导在 4.5 μm 波长 20 千瓦峰值功率下可以产生 3.0~12.2 μm(大于 2 倍频程)超连续谱, 这有利于片上超连续光源应用在生物医学成像、中红外环境和工业传感上。

关 键 词: ZnSe 脊波导; 超连续谱; 孤子自频移; 色散调制

Introduction

Supercontinuum (SC) generation in nonlinear materials excited by ultrashort pulses of peak power has raised great research interest, due to its wide applications in various fields [1]. This is especially evident in mid-infrared (MIR) SC sources, which have been used in sensing and detection of gas molecules, due to most of the gas molecules possessing intrinsic vibration absorption in the

Received date: 2020-12-15, **revised date**: 2021-04-21 **收稿日期**: 2020-12-15, **修回日期**: 2021-04-21

Foundation items: Supported by National Key R&D Program of China (2020YFB1805900), State Key Laboratory of Silicate Materials for Architectures (Wuhan University of Technology SYSJJ2019-09), National Natural Science Foundation of China (61775109), 3315 Innovation Team in Ningbo, K. C. Wong Magna 251 Fund in Ningbo University.

Biography: FANG Yi-Ming, female, Ningbo, China, master. Research area includings ZnSe materials and devices. E-mail: F691486627@163.com

* **Corresponding author**: E-mail: wangrongping@nbu.edu.cn

MIR [2-5]. In recent years, a wide variety of numerical and experimental investigations on mid-infrared supercontinuum generation were reported in fluoride glass [6], GaAs crystal [7], ZBLAN fiber [8], SiN waveguide [9], chalcogenide (ChG) planar waveguides [10-11] and fibers [12-13]. Wide transparency, high laser damage threshold, high optical nonlinearity of the materials, and suitable engineered dispersion in the waveguide or fiber structure are key factors to achieve broad SC spectra. Generally, SC generation requires the waveguide or fiber structure to be pumped by a laser with a wavelength near its zero-dispersion wavelength (ZDW) [14]. The ZDW of the fiber and planar waveguide structure can be finely tuned via adjusting the refractive index of the materials or structural parameters of the waveguide or optical fiber [15-17]. For example, in a 10-μm core step-index As_2Se_3 fiber, As_2Se_3 shows a material ZDW around 7 μm, which can be tailored to ~5 μm [15-16]. By tapering the As_2Se_3 fiber down to a diameter of 1.28 μm, the ZDW can also be further shifted to 1.73 μm [17]. Otherwise, by adjusting the structural parameters and cladding materials of $Ge_{11.5}As_{24}Se_{64.5}$ in the chalcogenide-glass channel waveguides, the zero dispersion point can be also shifted to different wavelengths [5].

Except for the adjustable ZDW in optical fiber, planar waveguide structures are also compatible with the well-developed semiconductor processing, which have better scalability and low fabrication cost. It has been demonstrated that supercontinuum spectra can be excited in ChG planar waveguides using a high peak power of few kW [18-20]. It is well known that high pump power is beneficial to broadening of supercontinuum spectrum since optical nonlinearity of the materials would be maximally excited under the high pump power. However, due to weak mechanical property and low laser damage threshold, ChG glasses are easily damaged under high pump power illumination, and this in turn limits the output power of SC generation [21-22]. ZnSe has a larger laser damage threshold around 1 300 mJ/cm^2 [23], which is nearly one or two orders of magnitude larger than the typical chalcogenide glasses [22, 24]. The large damage threshold indicates that higher peak power up to tens of kW is possible for supercontinuum generation in ZnSe waveguide. ZnSe with a broad transmission range from 0.5 to 22 μm has been widely used for the fabrication of mid-infrared optical components, such as optical lenses and windows [25]. Moreover, it has a reasonable high optical nonlinearity of 1.1×10^{-18} m^2/W [26] at 1.5 μm compared with a value of 2.9×10^{-18} m^2/W for typical As_2S_3 glass [27] at 1.5 μm, which is suitable for supercontinuum generation. Although SC generation from ZnSe bulk crystals has been reported [28-31] the ZnSe waveguides have been used in mid-infrared sensing [32-33], there is no reports on SC generation from a dispersion-engineered ZnSe waveguide as far as we know.

In this paper, we used ZnSe as core materials and simulated the dispersion, optical field distribution, the nonlinear coefficient, and effective mode area in the waveguide consisting of bottom and cladding layers with different thicknesses and refractive index contrast. Different cladding materials and waveguide structures affect the zero-dispersion wavelength. Furthermore, we numerically simulated SC generation in a 5-cm-long dispersion-engineered ZnSe rib waveguide pumped at different wavelength from 3 to 4.5 μm and different peak power from 100 W to 20 kW, and demonstrated a broadband SC spectrum from 3.0 to 12.2 μm in a 4-μm-width waveguide.

1 Simulation and discussion

The schematic diagram of the designed ZnSe rib waveguide is shown in Fig. 1 (a). The width 'w' of the waveguide is 4 μm or 8 μm. H_1 and H_2 represents ZnSe rib and ZnSe slab height, respectively. The refractive index of ZnSe [25] at a wavelength range from 2 to 10 μm is shown in Fig. 1 (b). The refractive index changes from 2.446 3 at 2 μm to 2.406 5 at 10 μm gradually. Previous experimental result has identified that $Ga_2As_{30}S_{68}$ has a refractive index of 2.25, while $Ge_5As_{10}S_{85}$ has a refractive index of 2.05 at 2 μm [34]. Therefore, it is much easier to design the cladding layer to achieve a refractive index contrast up to 0.4. For example by tuning the composition of S in cladding materials of GaAsS or GeAsS glasses during film deposition.

The Sellmeier equation used in the simulation of the

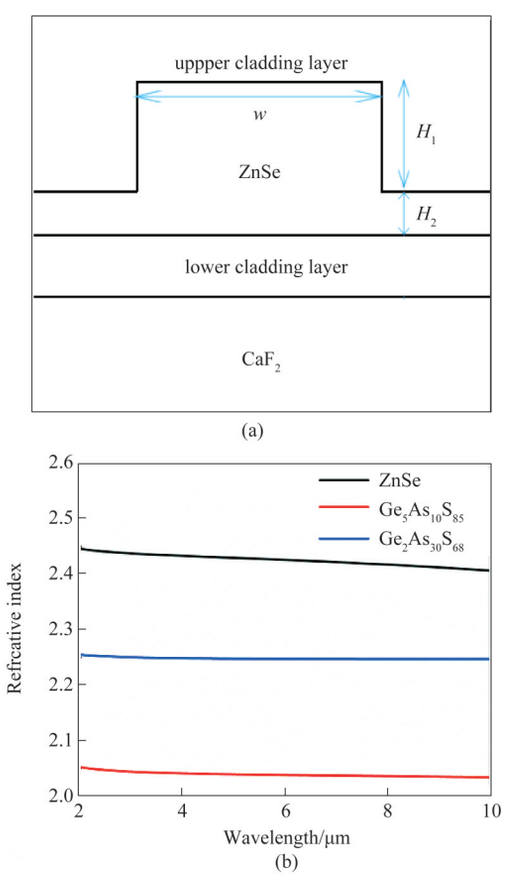

Fig. 1　(a) ZnSe waveguide structure, **(b)** refractive index of the core layer ZnSe, the cladding layer $Ga_2As_{30}S_{68}$ and $Ge_5As_{10}S_{85}$.
图 1　(a) ZnSe 波导结构，(b)ZnSe 芯层、$Ga_2As_{30}S_{68}$ 和 $Ge_5As_{10}S_{85}$覆盖层折射率

wavelength-dependent linear refractive index n over the entire wavelength range of ZnSe, $Ga_2As_{30}S_{68}$, and $Ge_5As_{10}S_{85}$ glass is given by Equation(1), where λ is the wavelength in micrometers, A_i and $\lambda_i^2 (i = 1, 2, 3)$ are material related constants, listed in Table1.

$$n(\lambda) = \sqrt{1 + \sum_{i=1}^{m} \frac{A_i \lambda^2}{\lambda^2 - \lambda_i^2}} \quad . \quad (1)$$

Table 1 Refractive coe ffi cient of ZnSe, $Ga_2As_{30}S_{68}$, and $Ge_5As_{10}S_{85}$.

表1 ZnSe、$Ga_2As_{30}S_{68}$和$Ge_5As_{10}S_{85}$的折射率系数

Materials	A_1	A_2	A_3	λ_1^2	λ_2^2	λ_3^2
ZnSe	4. 925 7	3. 247 7e^{-5}	22. 206 3	0. 051 3	19. 315	16 574
$Ga_2As_{30}S_{68}$	4. 044 5	1. 323 6e^{-4}	1. 282e^{-5}	0. 039 5	14. 107	29. 575
$Ge_5As_{10}S_{85}$	3. 154 6	−3. 007 5e^{-4}	−0. 058 1	0. 071 9	15. 124	−196. 7

The waveguide structures were optimized by using commercial software (COMSOL). With numerical analysis, the effective refractive index can be calculated by the Finite Element Modeling solver. Subsequently, the effective index was used for calculating the dispersion parameter as well as all other higher-order dispersion parameters.

The dispersion parameter curves of the modes can be calculated using:

$$D = -\left(\frac{\lambda}{c}\right) \cdot \left(\frac{\partial^2 n_{\text{eff}}}{\partial \lambda^2}\right) \quad , \quad (2)$$

here λ is the wavelength in micrometers, D is the dispersion parameter of the transmission mode, n_{eff} is the e ff ective refractive index of the fundamental mode and c is the light speed in vacuum. We investigated the dispersion of the waveguide, in which the top and bottom cladding layers were fixed at 2 μm, the total thickness of ZnSe film was 3 μm, and the ratio of H_1 to H_2 was variable.

Dispersion of the waveguide plays a significant role in SC generation. Ideally, dispersion near the pump wavelength should be anomalous as well as relatively flat[5]. Figure 2 (a) shows the dispersion of the fundamental quasi- transverse electric (TE) polarization in the waveguides with different structural parameters where the core-cladding refractive index contrast is kept around 0. 2 (employing $Ga_2As_{30}S_{68}$ glass for both the upper and lower claddings). It can be seen that, with the changing ratio of H_1 to H_2 and waveguide width, ZDW is always located at a longer wavelength more than 9 μm. It seems unlikely to shift ZDW to a shorter wavelength by employing such a lower refractive index contrast cladding material such as $Ga_2As_{30}S_{68}$ glass. To realize anomalous dispersion around the pump wavelength, increasing the refractive index contrast is essential. Figures. 2 (b-c) show the mapping of the calculated group velocity dispersion for TE polarization as functions of wavelength and thickness of H_1 in a waveguide with a width of 4 and 8 μm, respectively. In both cases, the core-cladding refractive index contrast is kept around 0. 4 (employing $Ge_5As_{10}S_{85}$ glass for both the upper and lower claddings), and the

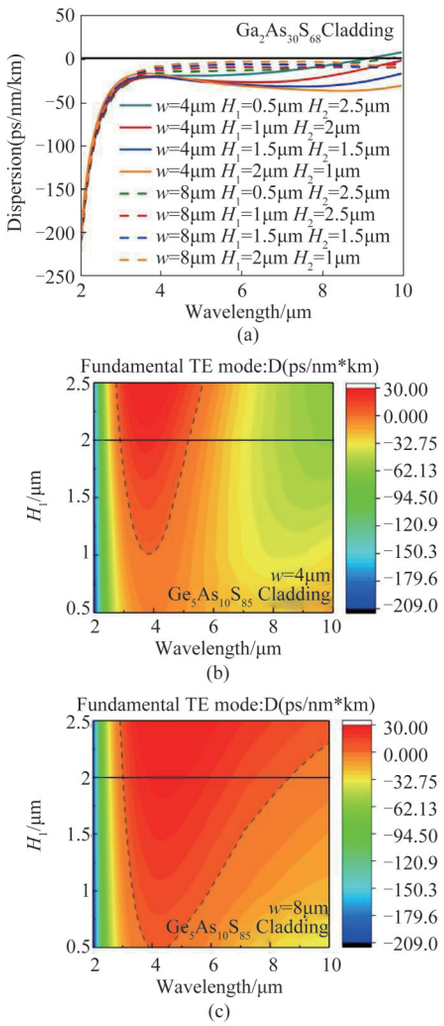

Fig. 2 Calculated dispersion curves of the fundamental quasi-TE (a) the dispersion parameter curves for the fundamental quasi-TE mode calculated from n_{eff} for eight waveguide geometries employing $Ga_2As_{30}S_{68}$ glass for both the upper and lower claddings, (b) and (c) Map of the dispersion parameter of w=4 and 8 μm ZnSe rib waveguides as a function of core thickness and wavelength, respectively, employing $Ge_5As_{10}S_{85}$ glass for both the upper and lower claddings. The dash lines show the change of the ZDWs

图2 TE基模的色散曲线 (a)采用$Ga_2As_{30}S_{68}$做包层的8种波导结构的有效折射率计算TE基模的色散,(b-c)上下包层为$Ge_5As_{10}S_{85}$ 4和8 μm宽不同结构的ZnSe脊波导色散图,虚线表示0色散点位置

ZDWs are tunable via changing parameter H_1. As H_1 increases, the overall dispersion gradually increases, and the anomalous dispersion appears when H_1 reaches 1 μm in Fig. 2 (b) and 0. 5 μm in Fig. 2 (c), respectively.

Therefore, all simulations in the rest part of the paper were performed in the waveguide with a refractive index contrast of 0. 4, since the larger refractive index contrast can tune the ZDW to a shorter wavelength as shown in Figs 2 (b) and (c). Moreover, we concentrated on the waveguides with the two typical structural parameters (w=4 μm, H_1=2 μm, H_2=1 μm and w=8 μm, H_1=2 μm, H_2=1 μm). The ZDWs can be seen as the cross-points in the solid and dash lines in Fig. 2 (b) and (c), respec-

tively. Both of them have the first ZDW around 3.0 μm, and the second ZDW at ~5 μm for the 4-μm-width waveguide and ~ 8.5 μm for the 8-μm-width waveguide.

Figures 3 (a-f) show the optical field distribution of the quasi-TE mode at different wavelengths in the waveguide with a width of 4 μm and 8 μm, respectively. It can be seen that, for the 4-μm-width waveguide, the light is well confined within the core as shown in Fig. 3 (a), slightly leaked to the cladding as shown in Fig. 3 (b), and considerably leaked out in Fig. 3 (c). For the 8-μm-width waveguide, the optical field distribution exhibits a similar feature with increasing wavelength, as shown in Figs. 3 (d-f), respectively. Comparing Fig. 3 (b) with (e), we can see that the light is better confined with increasing waveguide width since the waveguide width in Fig. 3 (b) is less than the wavelength of 6 μm. However, in both cases, the optical field is hardly leaked into the substrate layer even at 10 μm.

The nonlinear coefficient (Kerr effect), γ, which is determined by the effective mode area of the waveguide and the nonlinear refractive index of the material, can be calculated using the following formula,

$$\gamma = \frac{2\pi}{\lambda}\frac{n_2}{A_{\text{eff}}} \quad , \quad (3)$$

where n_2 is the nonlinear refractive index of ZnSe [26], A_{eff} is the effective area of the propagating mode, given by:

$$A_{\text{eff}} = \frac{\left(\int\int_{-\infty}^{+\infty}|E^2|\,\mathrm{d}x\mathrm{d}y\right)^2}{\left(\int\int_{-\infty}^{+\infty}|E|^4\,\mathrm{d}x\mathrm{d}y\right)} \quad , \quad (4)$$

where E is the electric field's transverse component propagating inside the waveguide.

The effective mode area and Kerr nonlinearity coefficient were calculated and shown in Fig. 4 (a-b), for the waveguide with a width of 4 μm and 8 μm, H_1=2 μm and H_2=1 μm, respectively. A general tendency is that as the nonlinear coefficient decreases, the effective area increases with increasing wavelength. However, the nonlinear coefficient is lower, but an effective area is larger in 8 μm-width waveguide compared with that in 4 μm-width one. This indicates that more power in the guided mode could enter the cladding as the wavelength increases, and thus the nonlinear coefficient gradually decreases [35], which is in agreement with the optical field distribution in Fig. 4.

We performed the simulations of SC generation by using a generalized nonlinear Schrödinger equation (GNLSE) with a chirp-free Gaussian-shaped pump pulse as the initial condition [36-37],

$$\frac{\partial}{\partial z}A(z,T) = -\frac{\alpha}{2}A + \sum_{k\geqslant 2}\frac{i^{k+1}}{k!}\beta_k\frac{\partial^k A}{\partial T^k} + i\left(\gamma + \frac{\alpha_2}{2A_{\text{eff}}}\right)\left(1 + \frac{i}{\omega 0}\frac{\partial}{\partial T}\right)\times\left(A(z,T)\int_{-\infty}^{\infty}R(T)\left|A(z,-T')\right|^2\mathrm{d}T'\right), \quad (5)$$

where A is the electrical field amplitude, $A(z,T)$ is the electric field wave amplitude as a function of propagation distance and time, $T=t-\frac{z}{v_g}$ is the retarded time frame moving at the group velocity $v_g=\frac{1}{\beta_1}$, α is the linear propagation loss of the waveguide including a wavelength-independent propagation loss of 0.6 dB/cm [32] for our 5-cm-long rib waveguides, $\beta_k(\omega)=\frac{\mathrm{d}^k\beta}{\mathrm{d}\omega^k}|_{\omega=\omega 0}(k\geqslant 2)$ is the k[th]-order dispersion parameter. The 10-order dispersion parameters are obtained by calculating the effective mode index with the finite-element method. And the nonlinear coefficient is $\gamma=\frac{n_2\omega_0}{cA_{\text{eff}}(\omega_0)}$, where n_2 is the nonlinear refractive index [26] and c is the speed of light in vacuum, $A_{\text{eff}}(\omega_0)$ is the effective area of the mode at the pump frequency ω_0, and α_2 = 5.5×10^{-14} m/W is the two-photon absorption coefficient [38]. Finally, the material response function includes both the instantaneous electronic response (Kerr type) and the delayed Raman response and has the form:

$$R(t) = (1-f_{\text{R}})\delta(t) + f_{\text{R}}h_{\text{R}}(t) \quad , \quad (6)$$

where the delayed Raman contribution $h_{\text{R}}(t)$ is given by:

$$h_{\text{R}}(t) = \frac{\tau_1^2+\tau_2^2}{\tau_1\tau_2^2}\exp\left(-\frac{t}{\tau_2}\right)\sin\left(\frac{t}{\tau_1}\right) \quad . \quad (7)$$

We calculated the Raman gain from the data available, and τ_1 and τ_2 from the linewidth of Raman spectrum of ZnSe, the response function coefficient f_{R} is 0.08, τ_1 is 21.06 fs, and τ_2 is 4.4 ps for ZnSe waveguide [39].

The GNLSE for the fundamental quasi-TE mode of the waveguides was calculated by using commercial software (MATLAB) to simulate SC generation. For numerical analysis of SC generation in a novel 5-cm-long dispersion engineered ZnSe rib waveguide, sub-femtosecond pulses with 150 fs duration and a repetition rate of 1 kHz were used as an exciting source.

Figures. 5-6 summarize the simulations of SC spectra with four different pump wavelengths for the two waveguides at different pump power. In Figs. 5 (a) and (c), when the pump wavelength is 3.0 μm, which is close to

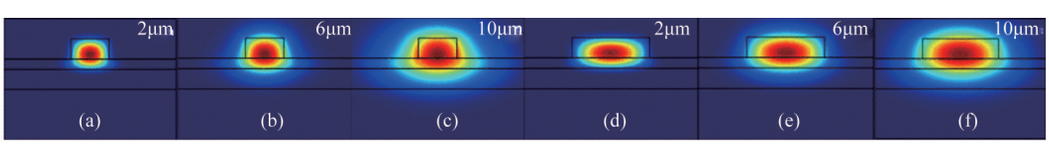

Fig. 3　The optical filed distribution for quasi-TE polarization in the waveguide (a-c) for w=4 μm, and (d-f) for w=8 μm waveguide with H_1=2 μm and H_2=1 μm at a wavelength of 2, 6, and 10 μm, respectively
图3　(a-c)宽4 μm和(d-f)宽8 μm, H_1=2 μm和H_2=1 μm的波导在2、6和10 μm波长处TE光场分布

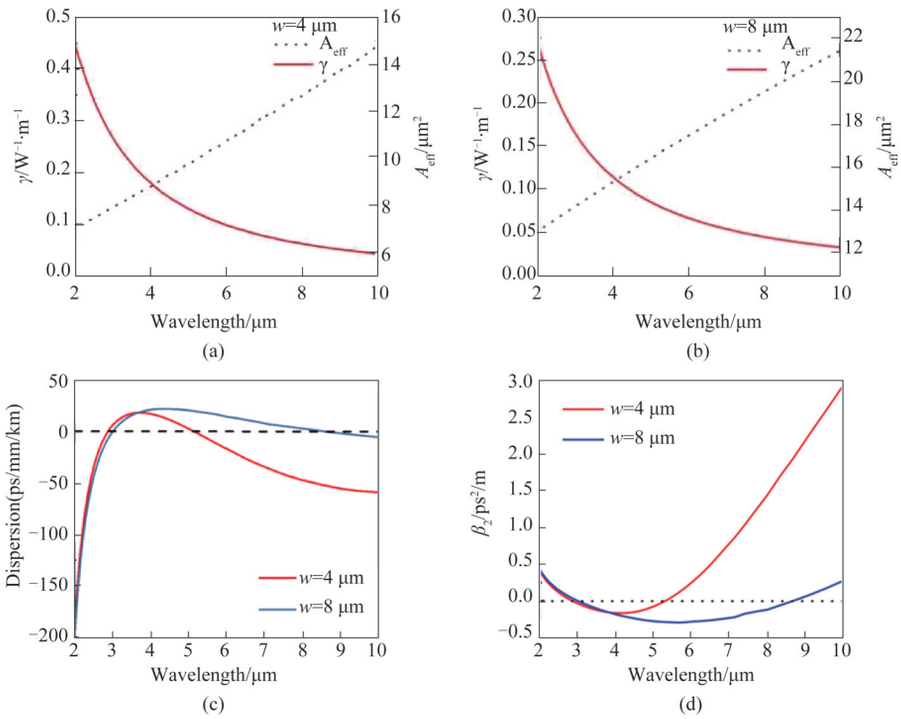

Fig. 4 Effective area and nonlinear coefficient of the fundamental mode calculated in the waveguides (a) w = 4 μm, H_1=2 μm, and H_2=1 μm (b) w = 8μm, H_1=2 μm, and H_2=1 μm. (c) Dispersion distribution of the waveguides with w = 4 and 8μm. (d) The second-order dispersion of the waveguides with w = 4 and 8 μm.

图4 计算波导基模有效面积和非线性系数(a) 宽4 μm (b) 宽8 μm, H_1=2 μm, H_2=1 μm。宽4和8 μm波导的(c)色散分布 (d) 二阶色散

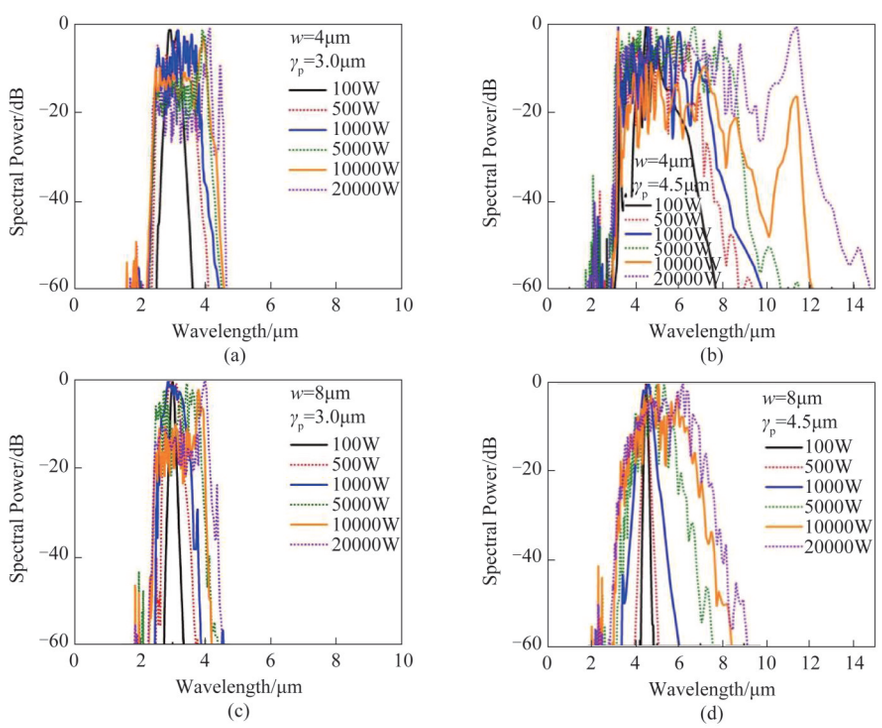

Fig. 5 Simulated SC spectra at a pump wavelength of (a) 3.0 μm, (b) 4.5 μm, (c) 3.0 μm and (d) 4.5 μm for the two waveguides at different peak power up to 20 kW, respectively.

图5 在泵浦波长为(a)3.0 μm (b)4.5 μm (c)3.0 μm和(d)4.5 μm的两个波导在不同峰值功率时的SC仿真光谱

the ZDWs of two waveguides, the change of the waveguide size has almost no effect on the spectral broadening. The SC bandwidth below -30 dB generally has a width from 2.6 μm (2.7 μm) to 3.4 μm (3.2 μm) in 4-

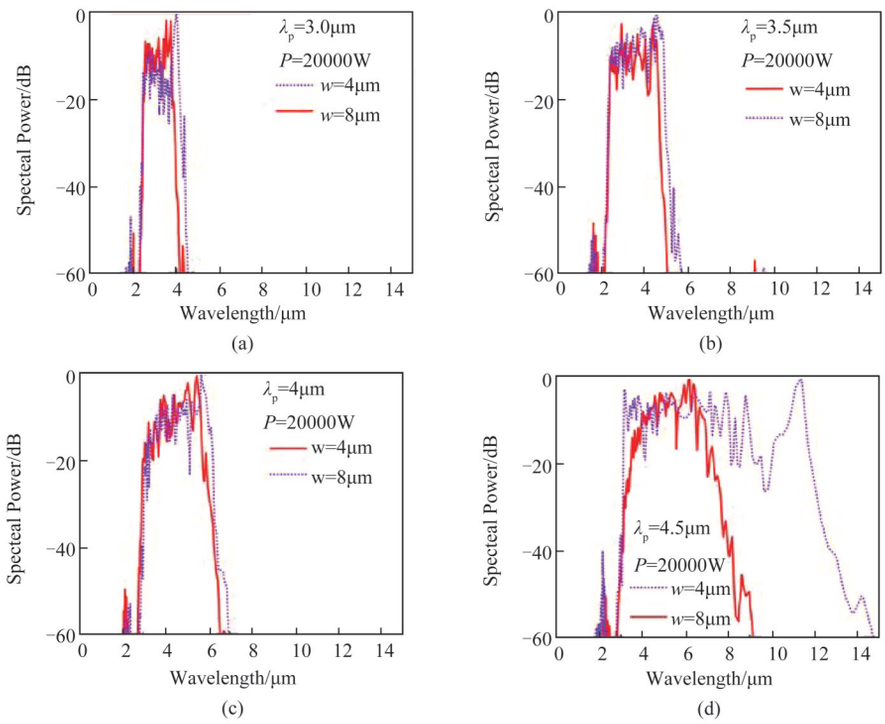

Fig. 6　Simulated SC spectra at different pump wavelengths of (a) 3.0 μm, (b) 3.5 μm, (c) 4.0 μm, and (d) 4.5 μm for the two waveguides with a peak power of 20 kW, respectively.
图6　两个波导在20 kW峰值功率不同泵浦波长(a)3.0 μm (b)3.5 μm (c)4.0 μm (d)4.5 μm的SC光谱

μm-width waveguide (in 8-μm-width waveguide) at 100 W, and slightly increases to a width from 2.3 μm (2.3 μm) to 4.6 μm (4.3 μm) at 20 kW. A significant difference can be found in Figs. 5(b) and (d) where the pump wavelength is 4.5 μm. SC spectrum generally broadens with increasing peak power. With a peak power of 20 kW, a bandwidth of 4.6 μm in 8-μm-width waveguide can be found compared with that of 9.2 μm in 4-μm-width waveguide below -30 dB.

For SC generation, self-phase modulation (SPM) alters the broadening rate imposed on the pulse by the group-velocity dispersion (GVD), and this has a correlation with the optical solitons in the abnormal dispersion region of the waveguide. The group velocity dispersion (β_2) in Fig. 4(d) is derived from the dispersion parameter in Fig. 4(c). From Fig. 4(d), since the value of β_2 is negative, the solitons are perturbed by high order dispersion and intrapulse Raman scattering and fission, and changed into multiple, much narrower, fundamental solitons, leading to the asymmetrical broadening of the spectrum. The present simulations demonstrated that the shift of the frequency of the solitons generated in abnormal dispersion region increases with increasing pump wavelength, and the edge of the solitons shifts to longer wavelength when the pump wavelength is from 3.0 to 4.5 μm as shown in Figs. 6(a-d). For sub-femtosecond pulses with a duration of 150 fs, its spectrum width is very wide, so that the blue-shifted spectrum component of the pulse can be used as a pump to effectively amplify the red-shifted component of the same pulse through Raman gain. Such a continuous process in the waveguide results in a constant energy transformation from the blue to the red component, as represented by the redshift of the soliton spectrum [40].

The spectral evolution corresponding to two curves in Fig. 6 (d) are shown in Fig. 7. For the 4-μm-width waveguide, it can be observed from Fig. 7 (a) that the SC extends over 9.2 μm covering a wavelength range from 3.0 μm to around 12.2 μm above 2 octaves. For the waveguide width is 8 μm, the SC extends over 4.6 μm covering a range from 3.1 μm to 7.7 μm above 1.3 octaves as shown in Fig. 7 (b). For the waveguides with different width of 4 μm and 8μm, the dispersion parameter D are 13.724 ps/nm/km and 22.863 ps/nm/km at 4.5 μm, respectively. The second-order dispersion $\beta_2 = -\frac{D\lambda^2}{2\pi c}$ = -0.1483 ps^2/m and -0.240 6 ps^2/m, and this leads to a dispersion length $L_D = \tau_P^2/|\beta_2|$ = 0.152 m and 0.093 m where τ_p is the laser pulse duration. Using the waveguide nonlinear parameter γ of 0.151 W^{-1}m^{-1} and 0.0965 W^{-1}m^{-1} for these two waveguides as shown in Fig. 4 (a) and (b), we obtained a nonlinear length L_{NL} at 20 kW of coupled power via $L_{NL} = 1/\gamma P$, being 0.331 mm and 0.520 mm, respectively. The soliton order $n_{sol} = \sqrt{L_D/L_{NL}}$ = 21.4 and 13.3.

When the dispersion length is comparable to the length of the waveguide, both GVD and SPM contribute to the formation of the solitons in the abnormal dispersion region [40]. When n_{sol} exceeds 1.5, the light pulses are transmitted as the second or higher-order solitons, and such the solitons undergo a splitting process if they are

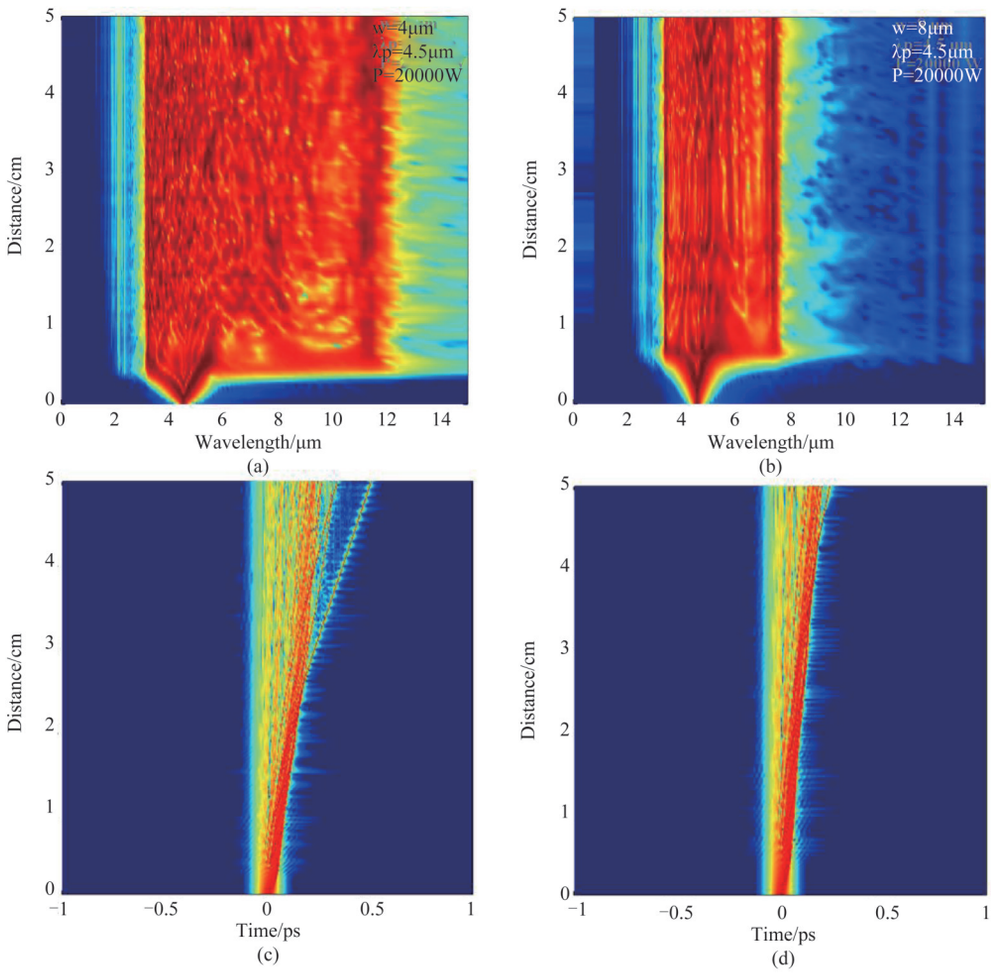

Fig. 7 The spectral evolution plots and temporal density plots corresponding to two curves in Fig. 5.2 (d) at a peak power of 20 kW for (a) the spectral evolution plot of 4 μm waveguide, (b) the spectral evolution plot of 8 μm waveguide, (c) the temporal density plot of 4 μm waveguide, (d) the temporal density plot of 8 μm waveguide.
图7 对应图5.2 (d) 20千瓦峰值功率的SC光谱和时间谱,(a)4 μm波导SC光谱,(b)8 μm波导SC光谱,(c)4 μm波导时间谱,(d)8 μm波导时间谱

disturbed by higher-order dispersion and intrapulse Raman scattering. n_{sol}-order solitons can produce N fundamental solitons and the frequencies of all the solitons are shorter than the original input pulse, and the shortest pulse width of the soliton is 1/(2N-1) of the input pulse width [40]. The pulse width of the soliton is around 3.6 fs and 6 fs, in 4 μm and 8μm-width waveguide, respectively. For an ultra-short pulse, its pulse width is opposite to its spectral width. With the assistance of Raman scattering process, the pulse spectrum toward longer wavelengths. A spectral shift can occur even in the normal-GVD regime of the waveguide where the solitons are not formed [40]. In the normal dispersion region, the pulse broadens rapidly while its spectrum is broadened through SPM. In contrast, in the anomalous dispersion region, the pulse slows down because the group velocity of a pulse is lower at longer wavelengths, and the SPM decreases the broadening rate [40]. Therefore, when the pump wavelength is 4.5 μm, the SC spectrum generated from 4-μm-width waveguide is broader than that from 8-μm-width waveguide, and the solitonic traces can be observed in the temporal density plots in Fig. 7(c-d), respectively.

2 Conclusion

We have numerically analyzed dispersion parameters, optical field distribution, nonlinear coefficient, and SC generation in ZnSe rib waveguide. It was found that ZDW can be shifted to shorter wavelength with increasing refractive index contrast between the core and cladding layer in the waveguide, and the optical field distribution can be well confined in 4- and 8-μm-width waveguide employing $Ge_5As_{10}S_{85}$ glass as both the upper and lower claddings. With increasing pump wavelength from 3.0 μm to 4.5 μm, SC spectrum broadens, and an ultrabroad SC spectrum can be obtained up to 9.2 μm (> 2 octaves) in a waveguide pumped by a peak power of 20 kW and a wavelength of 4.5 μm. Furthermore, the simulations confirm that the SC generation is initiated by self-phase modulation, followed by soliton dynamics and soliton self-frequency shift, both of which increase with increasing pump wavelength.

References

[1] Dudley J M, Taylor J R. *Supercontinuum generation in optical fibers* [M]. New York: Cambridge University Press, 2010

[2] Eggleton B J, Lutherdavies B, Richardson K. Chalcogenide photonics [J]. *Nature Photonics*, 2011, **5**:141-148

[3] Petersen C R, Møller U, Kubat I, *et al*. Mid-infrared supercontinuum covering the 1.4 - 13.3 μm molecular fingerprint region using ultra-high NA chalcogenide step-index fibre [J]. *Nature Photonics*, 2014, **8**:830

[4] Gao W Q, Amraoui E M, Liao M S,*et al*. Mid-infrared supercontinuum generation in a suspended-core As2S3 chalcogenide microstructured optical fiber [J]. *Optics Express*, 2013, **21**:9573

[5] Karim M R, Rahman B M , Agrawal G P. Mid-infrared supercontinuum generation using dispersion -engineered Ge (11.5) As (24) Se (64.5) chalcogenide channel waveguide [J]. *Opt Express*, 2015, **23**: 6903-6914.

[6] Liao M S, Gao W Q, Cheng T L, *et al*.Five-octave-spanning supercontinuum generation in fluride glass [J]. *App. Phy. Exp*, 2013, **6** (032503):1-3 .

[7] Pigeon J J, Tochitsky S Y, Gong C*et al*. Supercontinuum generation from 2 to 20 mum in GaAs pumped by picosecond CO(2) laser pulses [J]. *Opt Lett*, 2014, **39**:3246-3249.

[8] Kulkarni O P, Alexander V V, Kumar M, *et al*. Supercontinuum generation from 1.9 to 4.5 μm in ZBLAN fiber with high average power generation beyond 3.8 μm using a thulium-doped fiber amplifier [J]. J. *Opt. Soc. Am*. B,**2011 28**(10):2486 - 2498

[9] Porcel M A G, Schepers F, Epping J P, *et al*. Two-octave spanning supercontinuum generation in stoichiometric silicon nitride waveguides pumped at telecom wavelengths[J]. *Optics Express*,2017, **25**: 1542-1554

[10] Saini T S, Kumar A, Sinha R K. Design and modeling of dispersion engineered rib waveguide for ultra-broadband M-IR supercontinuum generation[J]. *Journal of Modern Optics*, 2017, **64**(2):143-149

[11] Karim M R, Ahmad H, Ghosh S*et al*. Design of dispersion-engineered As2Se3 channel waveguide for mid-infrared region supercontinuum generation editors-pick [J]. *J. Appl. Phys*, 2018, **123**: 213101

[12] Zhao Z M, Wang X S, Dai S X, *et al*. 1.5 - 14 μm midinfrared supercontinuum generation in a low-loss Te-based chalcogenide step-index fiber[J]. *Opt. Lett*, 2016, **41**:5222-5225.

[13] Zhao Z M, Wu B, Wang X S, *et al*. Mid-infrared supercontinuum covering 2.0-16 μm in a low-loss telluride single-mode fiber[J]. *Laser & Photonics Reviews*, 2017,**11**:1700005

[14] Yu Y, Gai X, Wang T, *et al*. Mid-infrared supercontinuum generation in chalcogenides[J]. *Optical Materials Express*, 2013, **3**:1075

[15] Dantanarayana H G, Abdel-Moneim N, Tang Z, *et al*. Refractive index dispersion of chalcogenide glasses for ultra-high numerical-aperture fiber for mid-infrared supercontinuum generation [J]. *Optical Materials Express*, 2014, **4**:1444

[16] Kubat I, Agger C S, Møller U, *et al*. Mid-infrared supercontinuum generation to 12.5μm in large NA chalcogenide step-index fibres pumped at 4.5μm[J]. *Opt. Express*,2014, **22**:19169-19182

[17] Al-kadry A, Baker C, Amraoui M E, *et al*. Broadband supercontinuum generation in As2Se3 chalcogenide wires by avoiding the two-photon absorption effects[J]. *Opt. Lett*, 2013, **38**:1185-1187.

[18] Yu Y, Gai X, Ma P, *et al*. Experimental demonstration of linearly polarized 2-10 mum supercontinuum generation in a chalcogenide rib waveguide[J]. *Opt. Let* , **2016 41**:958-961.

[19] Gai X, Choi D-Y, Madden S, Y, *et al*. Supercontinuum generation in the mid-infrared from a dispersion-engineered As2S3 glass rib waveguide[J]. *Opt. Lett*, 2012, **37**: 3870-3872.

[20] Al-kadry A, Amraoui M E, Messaddeq Y, *et al*. Two octaves mid-infrared supercontinuum generation in As2Se 3 microwires[J]. *Opt. Express*, 2014, **22**: 31131-31137

[21] Wang R P, Yan K L, Yang Z Y, *et al*. Structural and physical properties of Ge11.5As24S64.5·xSe64.5·(1 - X) glasses[J]. *Journal of Non Crystalline Solids*, 2015, **427**: 16-19.

[22] Li Q L, Qi D F, Wang X S, *et al*. Femto- and nano-second laser-induced damages in chalcogenide glasses[J]. *Japanese Journal of Applied*, 2019, **58**: 080911.

[23] Krola H, Grezes-Besset C, Gallais L, *et al*. Study of laser-induced damage at 2 microns on coated and uncoated ZnSe substrates [J]. *SPIE*,2006, **6403**:640316

[24] Ma W Q, Wang L L, Zhang P Q, *et al*. Surface damage and threshold determination of Ge - As - Se glasses in femtosecond pulsed laser micromachining [J]. *Journal of the American Ceramic Society* , 2020, 103(1) 94-102.

[25] The refractive index of ZnSe. Online at https://refractiveindex.info/?shelf=main&book=ZnSe&page=Connolly.

[26] Durand M, Houard A, Lim K, *et al*. Study of filamentation threshold in zinc selenide[J]. *Opt Express*, 2014, **22**:5852-5858.

[27] Wang T, Gai X, Wei W H, *et al*. Systematic z-scan measurements of the third order nonlinearity of chalcogenide glasses[J]. *Opt. Mater. Express*, 2014, **4**: 1011.

[28] Suminas R , Tamosauskas G, Valiulis G, *et al*. Multi-octave spanning nonlinear interactions induced by femtosecond filamentation in polycrystalline ZnSe[J]. *Appl Phys Lett*, 2017, **110**(241106):1-4

[29] Mouawad O, Bejot P, Billard F, *et al*. Filament-induced visible-to-mid-IR supercontinuum in a ZnSe crystal: Towards multi-octave supercontinuum absorption spectroscopy[J]. *Optical Materials*, 2016, **60**: 355.

[30] Werner K, Hastings M G, Schweinsberg A, *et al*. Ultrafast mid-infrared high harmonic and supercontinuum generation with n2 characterization in zinc selenide[J]. *Optics Express*, 2019, **27**(3):2867

[31] Suminas R, Marcinkeviciute A, Tamosauskas G*et al*. Even and odd harmonics-enhanced supercontinuum generation in zinc-blende semiconductors [J]. *Journal of the Optical Society of America B*, 2019,**36**(2):A22

[32] Mittal V, Sessions N P, Wilkinson J S, *et al*. Optical quality ZnSe films and low loss waveguides on Si substrates for mid-infrared applications[J]. *Optical Materials Express*, 2017, **7**: 712-745.

[33] Mittal V, Nedeljkovic M, Rowe D J, *et al*. Chalcogenide glass waveguides with paper-based fluidics for mid-infrared absorption spectroscopy[J]. *Opt. Lett*. 2018, **43**: 2913

[34] Borisova Z U. Glassy Semiconductors [M]. New York: Plenum Press,1981

[35] Zhu M, Liu H, Li X, *et al*. Ultrabroadband flat dispersion tailoring of dual-slot silicon waveguides [J]. *Optics Express*, 2012, **20**: 15899-15907.

[36] Karim M R, Rahman B M, Agrawal G P. Dispersion engineered Ge (1)(1).(5)As(2)(4) Se(6)(4).(5) nanowire for supercontinuum generation: a parametric study [J]. *Opt. Express*, 2014, **22**: 3102931040.

[37] Gai X, Madden S, Choi D-Y, *et al*. Dispersion engineered Ge11.5As24Se64.5 nanowires with a nonlinear parameter of 136W-1m-1 at 1 550 nm[J]. *Optics Express*, 2010,**18**: 18866-18874.

[38] Hutchings D C, Van Stryland E W. Nondegenerate two-photon absorption in zinc blende semiconductors[J]. *Journal of the Optical Society of America B*, 1992, **9**:2065-2074

[39] Anand S, Verma P, Jain K P, *et al*. Temperature dependence of optical phonon lifetimes in ZnSe[J]. *Physica B*, 1996, **226**:331-337

[40] Agrawal G. *Nonlinear fiber optics* [M]. New York: Elsevier Press, 2013.